Experimental and theoretical investigation of the $H\bar{H}\,^1\Sigma_g^+$ state in H_2, D_2, and HD, and the $B''\bar{B}\,^1\Sigma_u^+$ state in HD

E. Reinhold, W. Hogervorst, and W. Ubachs
Department of Physics and Astronomy, Vrije Universiteit, De Boelelaan 1081, 1081 HV Amsterdam, The Netherlands

L. Wolniewicz
Nicholas Copernicus University, 87-100 Torun, Poland
(Received 19 January 1999)

We present an extensive experimental and theoretical study of the energy levels of the $\bar{H}$ outer-well part of the $H\bar{H}\,^1\Sigma_g^+$ state, which is the fourth adiabatic state of $^1\Sigma_g^+$ symmetry in the hydrogen molecule. Experimentally, rovibrational $\bar{H}$ levels were excited in a two-step laser excitation, using wavelength tunable extreme ultraviolet radiation near 91 nm to prepare selected levels in the $B\,^1\Sigma_u^+$ state ($v=18$ and 19 for H_2 and $v=25$–27 for D_2, $v=21$–23 for HD). A second tunable laser in the range 550–735 nm was used to excite the $\bar{H}$ levels in the isotopomers H_2, D_2, and HD. A third laser at 355 nm probed the excitation of the $\bar{H}$ levels by dissociative ionization, producing ions for signal detection. For H_2 82 quantum levels were calibrated ($v=2$–15, $J=0$–5) and 107 levels for D_2 ($v=6$–22, $J=0$–5). These level energies are compared with *ab initio* calculations including adiabatic and relativistic effects. Agreement between observation and calculation is of the order of 1 cm^{-1} for H_2 and 0.5 cm^{-1} for D_2 throughout the rovibrational manifold. In the HD isotopomer the $\bar{H}\,^1\Sigma_g^+$ state nonadiabatically interacts with the $\bar{B}\,^1\Sigma_u^+$ state. This mixing represents an example of strong *g*-*u* symmetry breaking. Apart from $\bar{H}$ levels ($v=4$–19, $J=0$–3) also $\bar{B}$ levels ($v=9$–20, $J=0$–3) were observed. Theoretical results for HD account for the nonadiabatic interaction with the $\bar{B}$ state, based on a new *ab initio* calculation of the $B''\bar{B}\,^1\Sigma_u^+$ potential and the coupling with the $H\bar{H}\,^1\Sigma_g^+$ state. Except for some levels near the potential barrier also for HD the experimentally calibrated levels agree with the *ab initio* calculated energies within 1.5 cm^{-1}. [S1050-2947(99)06007-2]

PACS number(s): 33.80.Rv, 31.15.Ar, 31.50.+w, 11.30.−j

I. INTRODUCTION

Spectroscopy of the hydrogen molecule has been of fundamental interest since the early days of quantum mechanics. Hydrogen, being the smallest neutral molecule, is considered the ideal test system for quantum chemical *ab initio* calculations of energy levels in a bound molecular system. It may be argued that the hydrogen molecule is not the simplest system since the low mass of the nuclei gives rise to strong deviations from the Born-Oppenheimer approximation; from that perspective the theoretical calculations on the hydrogen molecule may serve as a test for an understanding of such effects. As for the $X\,^1\Sigma_g^+$ ground state of H_2 and its isotopomers D_2 and HD energy levels have been calculated with an accuracy of 0.01 cm^{-1}, where nonadiabatic, relativistic, and radiative (Lamb shift) corrections were included [1,2]. These calculations on the binding energy of the $X\,^1\Sigma_g^+$ ground state have been tested in several experiments determining its dissociation energy [3–6]. Discrepancies between theory and experiment have reached a level of a few hundredths of a wave number. The values obtained for the ionization potentials of hydrogen and its isotopomers [7,8] are as accurate as 0.01 cm^{-1}. The excited states of $^1\Sigma_g^+$ symmetry were theoretically investigated with increasing accuracies over the last decade [9,10]. Recently some nonadiabatic [11] and relativistic corrections [12] for the lowest $^1\Sigma_g^+$ states were computed as well. Calculations for the lowest vibrational levels in the second adiabatic state of $^1\Sigma_g^+$ symmetry, the $EF\,^1\Sigma_g^+$ state, now have reached agreement with experiment within 0.1 cm^{-1}. Ross and Jungen [13] have developed an alternative theoretical framework, that of multichannel quantum defect theory (MQDT), from which level energies can be computed as well; in case of the $EF\,^1\Sigma_g^+$ state accuracies on the order of several cm^{-1} have been achieved.

Potentials of the hydrogen molecule show complicated shapes as a function of the internuclear distance due to avoided crossings between diabatic energy curves, belonging to singly and doubly excited molecular configurations as well as superpositions of atomic states. A celebrated example of a double-well structure is that of the above-mentioned $EF\,^1\Sigma_g^+$ state, which was observed by Davidson [14]. Both inner- and outer-well states were subsequently probed by two-photon laser excitation [15]. Details of the tunneling dynamics in this system were theoretically investigated by Dressler and co-workers [16,17]. The third adiabatic state of $^1\Sigma_g^+$ symmetry, denoted as $GK\,^1\Sigma_g^+$, has a somewhat less-pronounced double-well structure as well [18].

For the fourth potential of the $^1\Sigma_g^+$ manifold, called $H\bar{H}$, it has been predicted that a secondary minimum at 11 a.u. must exist [19], which is due to a crossing between the $H^+ + H^-(1s)^2$ ion-pair configuration and a repulsive $H(1s) + H(2p)$ Heitler-London configuration. The latter develops into the doubly excited molecular $2p\sigma_u 3p\sigma_u$ state at smaller internuclear distance R; a barrier is formed by an avoided crossing with Rydberg configurations, forming a typical

bound excited state at short R, the $H\ ^1\Sigma_g^+$ state. Energy levels in the H inner-well structure have been investigated by Tsukiyama and co-workers for H_2 as well as D_2 [20,21].

The first observation of the outer-well $\overline{H}$ state in H_2 [22] resulted in an experimental determination of rovibronic level energies that agreed with predictions from *ab initio* theory [23] within 13–20 cm^{-1}. More recently a recalculation of the Born-Oppenheimer potential for a wide range of internuclear distances, including adiabatic shifts and relativistic effects [12,24], reduced this difference between theoretical and experimental level energies in H_2 by more than one order of magnitude, as shown in detail in this paper. The same calculation can be applied to D_2, and results are also compared with experimental data. However, strong deviations from adiabatic energies occur in HD.

The case of the HD isotopomer is qualitatively different from that of the symmetric H_2 and D_2 molecules: the inversion symmetry, which still holds in the Born-Oppenheimer approximation, is dynamically broken by asymmetric nuclear motion. Electronic states of gerade and ungerade symmetry are mixed, thus lowering the electronic symmetry from $D_{\infty h}$ to $C_{\infty v}$, and g-u dipole selection rules do not strictly apply any more to electronic transitions. Due to the large H:D mass ratio, in HD this effect is strongest among all diatomic molecules. The observation of a very weak vibrational spectrum in HD [25] provided evidence for a static electric dipole moment and a deviation from inversion symmetric charge distribution in the electronic ground state. Wave function mixing between $EF\ ^1\Sigma_g^+$ states on the one hand and $B\ ^1\Sigma_u^+$ and $C\ ^1\Pi_u$ states on the other, observed as line shifts and the appearance of additional lines in the extreme ultraviolet (XUV) absorption spectrum, provide further evidence [26,27]. But in these examples the symmetry-breaking effect was small, except for some special cases of near resonance, and g and u can still be used as approximate quantum numbers.

In a recent Letter [28] strong g-u symmetry breaking was reported for the $H\overline{H}\ ^1\Sigma_g^+$ state of HD. For entire rotational manifolds within a progression of vibrational states in the $H\overline{H}\ ^1\Sigma_g^+$ state strong mixing with the $B''\overline{B}\ ^1\Sigma_u^+$ state was observed. In Fig. 1 potential energy curves of both states are shown. The mixing was analyzed semiempirically, considering a strong perturbation that acts on undisturbed $\overline{H}$ levels constructed on the basis of Dunham coefficients calculated from the H_2 and D_2 isotopomers.

Here we present an *ab initio* study of the strongly interacting $\overline{H}$ and $\overline{B}$ states in HD and a detailed comparison with experimental results. For this purpose the $B''\overline{B}\ ^1\Sigma_u^+$ Born-Oppenheimer potential and adiabatic corrections were calculated, and the nonadiabatic contributions from the symmetry-breaking term in the Hamiltonian were computed to obtain a full set of rovibronic energy levels for the interacting $H\overline{H}\ ^1\Sigma_g^+$ and $B''\overline{B}\ ^1\Sigma_u^+$ systems. Inclusion of this nonadiabatic interaction term in the theory provides a special test for the *ab initio* theory of this molecule.

II. THEORETICAL RESULTS

In two recent papers a recalculation of the Born-Oppenheimer potential for the $H\overline{H}\ ^1\Sigma_g^+$ state of H_2 was reported including adiabatic and relativistic effects [12,24]; these results can be extended to D_2 in a straightforward way. For the purpose of calculating levels in HD, first the $B''\overline{B}\ ^1\Sigma_u^+$ Born-Oppenheimer potential and adiabatic corrections were recalculated; then the electronic coupling between the $B\overline{B}$ and $H\overline{H}$ states was evaluated, and finally vibrational levels were calculated.

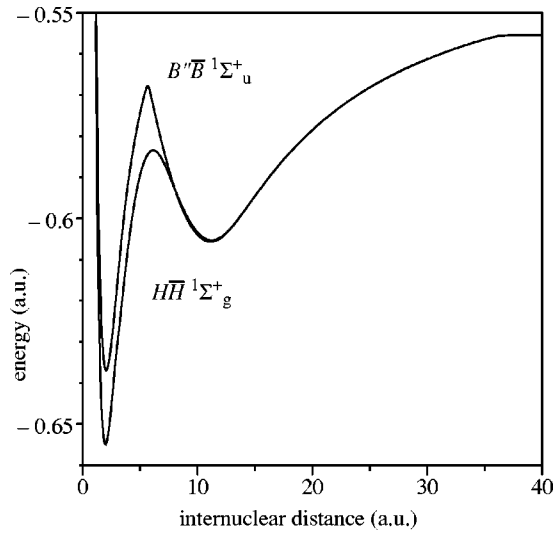

FIG. 1. Born-Oppenheimer potentials for the $H\overline{H}$ and $B''\overline{B}$ states of the hydrogen molecule; the former taken from Ref. [24], the latter from the present calculation.

A. Adiabatic potentials

Similarly as in the case of the $H\overline{H}$ state, the outer minimum of the $B''\overline{B}$ Born-Oppenheimer potential, for which a calculation was reported by Kołos [29], is due to an avoided crossing of a repulsive Heitler-London and an attractive ionic configuration. As a consequence, the wave function in the outer minimum is a superposition of two components: covalent and ionic. Therefore, in order to compute the adiabatic potential correctly, we applied the same procedure recently used for the $H\overline{H}$ state [24]. Except for the change in symmetry, both components of the wave function were defined with the same 299 terms as in Ref. [24], i.e., the total wave function consisted of 598 terms. The nonlinear parameters were reoptimized.

The accuracy was secured in the same way as in Ref. [24] and double precision floating point arithmetic was used for internuclear distances $R>30$ a.u. For $R>3.0$ a.u. the present energies are lower than those in Ref. [30]. Therefore the adiabatic potential was recomputed at about 260 internuclear distances in the interval $3<R\leqslant 40$ a.u. Tests performed at several selected internuclear distances have shown that a more careful selection of terms could still improve the energies by a few hundredths of a wave number. However, this convergence error is definitely smaller than the neglected nonadiabatic and relativistic corrections. We list some of the results in Table I. For consistency with earlier convention, the adiabatic correction is listed for H_2; values for HD or D_2 are obtained by scaling with the inverse of the reduced mass of nuclear motion.

The large R behavior of the potential and adiabatic correction is very similar to that of the $H\overline{H}$ state [24] and the

TABLE I. $B''\overline{B}$ state: Born-Oppenheimer potential and adiabatic correction for H_2.

R (a.u.)	E_{BO} (a.u.)	dE/dR	$D(\mathrm{cm}^{-1})$[a]	Δ_{old}[b]	$\langle H' \rangle$[c]
3.10	−0.612 756 808 1	0.029 389 824 5	12 554.22	−0.05	97.64
3.70	−0.596 666 238 2	0.023 496 282 5	9022.75	−0.79	100.82
4.00	−0.590 154 894 0	0.019 999 519 5	7593.68	−0.95	97.92
5.00	−0.574 148 641 5	0.0128 299 528	4080.71	−0.74	75.05
5.60	−0.567 847 333 1	0.004 713 075 9	2697.73	−3.53	1912.98
5.70	−0.567 885 627 8	−0.005 838 416 6	2706.14	−7.07	2583.15
6.00	−0.571 113 046 7	−0.012 211 938 0	3414.47	−3.05	123.63
6.50	−0.577 231 165 8	−0.011 997 280 9	4757.25	−0.55	97.59
7.00	−0.583 001 729 8	−0.011 025 527 0	6023.74	−0.40	92.57
8.00	−0.592 774 254 0	−0.008 425 997 3	8168.56	−0.67	86.66
9.00	−0.599 787 247 9	−0.005 607 244 5	9707.73	−1.13	83.08
10.00	−0.604 035 782 3	−0.002 911 994 1	10 640.18	−1.79	80.94
11.00	−0.605 645 569 7	−0.000 324 445 2	10 993.49	−2.78	79.59
11.10	−0.605 665 547 6	−0.000 074 411 2	10 997.87		79.43
11.20	−0.605 660 679 3	0.000 172 420 3	10 996.80	−2.89	79.25
12.00	−0.604 784 473 2	0.001 947 0273	10 804.50	−2.68	76.99
13.00	−0.602 052 402 5	0.003 346 278 0	10 204.88	−3.34	72.88
14.00	−0.598 398 254 5	0.003 845 386 4	9402.89	−3.98	69.89
15.00	−0.594 528 174 9	0.003 843 211 1	8553.50	−4.32	68.34
16.00	−0.590 780 208 9	0.003 634 996 5	7730.92	−4.32	67.56
18.00	−0.584 064 676 4	0.003 075 792 9	6257.03	−4.46	66.95
20.00	−0.578 447 122 2	0.002 558 108 5	5024.12	−3.77	66.77
22.00	−0.573 771 954 5	0.002 134 256 4	3998.04	−3.75	66.73
24.00	−0.569 856 248 8	0.001 796 071 7	3138.64	−4.41	66.75
30.00	−0.561 274 738 1	0.001 137 033 7	1255.22	−7.90	66.86
33.00	−0.558 186 979 8	0.000 931 114 5	577.53		66.93
36.00	−0.555 757 516 8	0.000 466 152 1	44.33		196.12
36.10	−0.555 715 194 8	0.000 380 340 6	35.04		205.03
36.20	−0.555 681 426 9	0.000 296 819 2	27.63		189.91
40.00	−0.555 559 789 9	0.000 001 152 9	0.93		68.93

[a]BO dissociation energy.
[b]Energy improvement over best previous, results in cm^{-1} [30]. 1 a.u.$=219\,474.631$ cm^{-1}.
[c]Total adiabatic correction for H_2; values for the other isotopes are obtained by scaling with $1/\mu$, μ being the reduced mass of nuclear motion.

changes in character from ionic to covalent are best visible in the adiabatic corrections and the slope of the Born-Oppenheimer potential, dE/dR.

B. Electronic coupling

The total Hamiltonian (see, e.g., Ref. [1]) is

$$H=H_c+H_1+H_2+H_3, \tag{1}$$

where H_c is the clamped nuclei Hamiltonian and

$$H_1=-(1/2\mu)\Delta_R, \tag{2}$$

$$H_2=-(1/8\mu)(\nabla_1+\nabla_2)^2, \tag{3}$$

$$H_3=-(1/2\mu_a)\nabla_R\cdot(\nabla_1+\nabla_2). \tag{4}$$

Above, 1 and 2 denote the electrons, R the internuclear distance $|\mathbf{R}_A-\mathbf{R}_B|$, μ is the reduced mass of the nuclei, $1/\mu_a=1/M_B-1/M_A$, and A,B denote the two nuclei, respectively.

In general, H_1 and H_2 give rise to adiabatic corrections and to nonadiabatic couplings between states of the same g,u symmetry. The symmetry-breaking term, H_3, which is a consequence of the fact that the nuclear center of mass does not coincide with the geometrical center of the molecule, is responsible for the g-u coupling. In the present work we are interested in the anomalies in the HD spectrum that are primarily due to strong interactions between nearby $B''\overline{B}$ and $H\overline{H}$ vibrational levels. Therefore we concentrate on this interaction and ignore all others.

In the following the electronic functions of the $B''\overline{B}$ and $H\overline{H}$ states will be denoted by ψ_1 and ψ_2, respectively. For Σ symmetry, with the molecule fixed z axis coinciding with the internuclear separation vector $\mathbf{R}$, the electronic matrix elements describing the coupling are thus

$$\left(\psi_i\left|RH_3\frac{1}{R}\right|\psi_k\right)=-(1/\mu_a)\left(A_{i,k}+B_{i,k}\frac{d}{dR}\right), \quad i\neq k \tag{5}$$

where

TABLE II. $B''\overline{B}$-$H\overline{H}$ nonadiabatic coupling parameters as defined in Eqs. (6) and (7); all values in atomic units.

R	$A_{1,2}$[a]	$B_{1,2}$[b]	$A_{2,1}$	R	$A_{1,2}$	$B_{1,2}$	$A_{2,1}$
1.100	0.027 12	−0.042 17	0.046 76	20.000	0.277 54	0.000 01	0.277 55
1.400	0.026 06	−0.047 68	0.042 69	22.000	0.278 05	0.000 00	0.278 05
2.000	0.025 20	−0.054 08	0.028 35	24.000	0.278 44	0.000 00	0.278 44
2.400	0.025 80	−0.052 72	0.014 68	28.200	0.279 03	0.000 01	0.279 03
2.800	0.072 65	−0.040 61	0.001 54	30.900	0.278 50	0.000 31	0.278 47
2.850	0.093 99	−0.036 51	0.000 60	34.700	0.276 06	0.000 65	0.275 49
2.900	0.116 23	−0.031 26	0.000 06	35.930	0.228 39	0.002 61	0.224 62
3.000	0.127 32	−0.018 56	0.000 23	35.980	0.222 88	0.002 76	0.219 22
3.050	0.111 40	−0.012 58	0.000 70	36.031	0.216 63	0.002 90	0.213 89
3.100	0.090 96	−0.007 57	0.001 23	36.036	0.213 71	0.002 91	0.212 90
3.150	0.072 19	−0.003 59	0.001 74	36.039	0.206 51	0.002 90	0.211 51
3.200	0.057 18	−0.000 48	0.002 28	36.040	0.199 63	0.002 89	0.210 48
3.400	0.026 51	0.006 57	0.004 37	36.041	0.188 63	0.002 87	0.209 09
3.600	0.017 22	0.009 58	0.007 26	36.043	0.106 94	0.002 77	0.201 27
3.800	0.015 30	0.010 88	0.011 54	36.046	−0.415 89	0.001 69	0.123 31
4.000	0.017 06	0.011 21	0.017 09	36.047	−0.289 83	0.001 21	0.088 89
4.600	0.034 05	0.009 54	0.037 97	36.050	−0.062 05	0.000 57	0.042 30
5.000	0.050 78	0.008 21	0.053 06	36.052	−0.025 22	0.000 41	0.030 98
5.200	0.061 64	0.007 88	0.062 37	36.056	−0.003 43	0.000 26	0.020 26
5.400	0.079 61	0.007 91	0.078 49	36.057	−0.001 25	0.000 24	0.018 73
5.600	0.140 10	0.007 70	0.149 57	36.060	0.002 36	0.000 19	0.015 48
5.650	0.173 60	0.006 71	0.202 54	36.062	0.003 37	0.000 17	0.013 52
5.700	0.199 73	0.004 82	0.239 77	36.064	0.004 05	0.000 15	0.012 29
5.750	0.210 82	0.002 89	0.244 74	36.068	0.004 67	0.000 13	0.010 41
5.800	0.214 94	0.001 33	0.241 01	36.071	0.004 92	0.000 11	0.009 51
6.000	0.219 51	−0.001 89	0.231 21	36.078	0.004 79	0.000 09	0.007 72
6.100	0.221 11	−0.002 86	0.228 97	36.080	0.003 37	0.000 05	0.005 07
6.400	0.224 41	−0.004 08	0.225 57	36.200	0.001 50	0.000 03	0.001 70
6.500	0.225 04	−0.004 13	0.224 89	36.300	−0.000 10	0.000 02	0.000 00
7.000	0.225 42	−0.003 11	0.222 27	36.400	−0.001 67	0.000 02	−0.001 59
8.000	0.220 74	−0.000 11	0.218 47	36.500	−0.003 34	0.000 01	−0.003 27
9.000	0.218 58	0.001 34	0.217 82	36.600	−0.005 12	0.000 01	−0.005 06
10.000	0.221 77	0.001 67	0.221 78	36.700	−0.007 08	0.000 01	−0.007 02
11.000	0.231 51	0.001 44	0.231 93	36.800	−0.009 18	0.000 00	−0.009 12
12.000	0.246 78	0.000 93	0.247 32	37.000	−0.013 90	0.000 00	−0.013 85
14.000	0.269 12	0.000 22	0.269 29	38.000	−0.050 42	0.000 00	−0.050 41
16.000	0.275 15	0.000 06	0.275 19	39.000	−0.100 10	0.000 02	−0.100 11
18.000	0.276 80	0.000 02	0.276 81	40.000	−0.130 31	0.000 03	−0.130 33

[a]Index 1 corresponds to the $B''\overline{B}$ state.
[b]$B_{2,1}=-B_{1,2}$.

$$A_{i,k}=\left(\psi_i\left|\frac{\partial^2}{\partial z_1\partial R}\right|\psi_k\right) \tag{6}$$

and

$$B_{i,k}=\left(\psi_i\left|\frac{\partial}{\partial z_1}\right|\psi_k\right). \tag{7}$$

Above, we use the $(\ldots|\ldots)$ notation to denote integrals over electronic coordinates, and z_1 is the molecule fixed z coordinate of one of the electrons. To compute in single precision floating point arithmetic the matrix elements $A_{i,k}$ and $B_{i,k}$ we used different variational wave functions for small and large internuclear distances. For $R\leqslant 30$ a.u. we used the $H\overline{H}$ state function of Ref. [24] and for the $B''\overline{B}$ states, for $R\leqslant 3$ a.u. the wave functions of Ref. [30], and for $3<R\leqslant 30$ a.u. the function computed in this work. For $30<R\leqslant 40$ a.u., because of numerical instabilities, we had to use shorter expansions and the number of terms was reduced from 299 to 50 for both the ionic and covalent components. This results in a discontinuity of the matrix element $B_{1,2}$ but has no effect on the final results due to the smallness of $B_{1,2}$. This can be seen in Table II where we list the coupling elements for some internuclear distances. (A complete set of results can be obtained from the authors [31].) Strong nonadiabatic couplings, due to avoided crossings with other po-

tentials, are clearly visible in the vicinity of $R=3$, 6, and 36 a.u. Since both states dissociate to the same limit, $A_{i,k}$ and $B_{i,k}$ vanish at infinite separations. The results in Table II show that at $R=40$ a.u. the asymptotic region has not yet been reached. This is in agreement with the results of Ref. [24].

C. Vibrational levels

The adiabatic potentials of the $B''\overline{B}$ and $H\overline{H}$ states and the nonadiabatic couplings between these states were used to determine the vibrational levels with a variational procedure. The basis functions were assumed in the form of products, $\psi_i F_{i,v}(R)$, where $i=1,2$, $v=0,\ldots,v_{\max}$, and ψ_i and $F_{i,v}$ are the electronic and adiabatic vibrational-rotational functions of the $B''\overline{B}$ and $H\overline{H}$ states, respectively. Thus the total wave function is given as

$$\Psi=\frac{1}{R}\sum_{i=1}^{2}\sum_{v=0}^{v_{\max}} c_{i,v}\psi_i F_{i,v} \tag{8}$$

and the matrix elements of the Hamiltonian, Eq. (1), are

$$\langle i,v|H|i,v'\rangle=\delta_{v,v'}E_{i,v}^{\mathrm{ad}}, \tag{9}$$

$$\langle i,v|H|k,v'\rangle=-(1/\mu_a)\left(\int F_{i,v}A_{i,k}F_{k,v'}dR + \int F_{i,v}B_{i,k}\frac{d}{dR}F_{k,v'}dR\right),\quad i\neq k \tag{10}$$

with $E_{i,v}^{\mathrm{ad}}$ being the corresponding adiabatic vibration-rotational energy. The adiabatic vibrational functions were computed with the boundary conditions $F(0)=F(40)=0$ to allow for levels above the dissociation limit. The differentiation of the adiabatic vibrational functions was performed numerically.

In the final computations we used $v_{\max}=120$ which resulted, for each electronic state, in about 40 levels corresponding to the continuum. A reduction of the basis to $v_{\max}=100$ changed the final energies by not more than 0.01 cm^{-1}. We list the final term values in Table III. These were obtained with the assumption that the relativistic correction to the vibrational levels is equal to that of the separated atoms.

The probability of finding the electronic state ψ_i is

$$P_i=\sum_v |c_{i,v}|^2. \tag{11}$$

If $P_1\geqslant P_2$ the corresponding term in Table III is denoted by B (inner-well $B''\overline{B}$ states) or $\overline{B}$ (outer-well $B''\overline{B}$ states); otherwise by H or $\overline{H}$, respectively.

Within the two-state model, the final results listed in Table III are accurate to a hundredth of a wave number. The errors are due to inaccuracies in the adiabatic potential and in the variational solution of the coupled vibrational equations. However, the neglected nonadiabatic corrections due to interactions with states of the same g,u symmetry and relativistic corrections are certainly much larger and amount probably to about one wave number, or more. It seems plausible that the relativistic corrections to the $B''\overline{B}$ state are similar to those to the $H\overline{H}$ state. Therefore one would expect that relativistic effects would raise the term values in Table III by about 0.3 cm^{-1} [12]. The neglected nonadiabatic corrections can — at this moment — only be estimated by a comparison with accurate experimental data.

III. EXPERIMENT

$\overline{H}\,^1\Sigma_g^+$ levels cannot be excited directly from the $X\,^1\Sigma_g^+$ ground state of the hydrogen molecule because there is no Franck-Condon overlap due to the large internuclear distance of the $\overline{H}$ state . Therefore we excited $\overline{H}\,^1\Sigma_g^+$ rovibronic levels in a resonance-enhanced two-photon transition scheme, using $B\,^1\Sigma_u^+$ vibronic states as intermediates, thereby bridging the gap in internuclear distance between the X and $\overline{H}$ vibrational wave functions. Population of excited $\overline{H}$ levels is probed by ionization with a third laser pulse. This scheme for the optical excitation is shown in Fig. 2. The $\overline{B}\,^1\Sigma_u^+$ state in HD is excited in the same way, using also $EF\,^1\Sigma_g^+$ levels as intermediates.

The experiment has been briefly described in a previous Letter [22] and in a report on the observation of the $I'\,^1\Pi_g$ state of hydrogen [32]. In Fig. 3 the experimental setup is shown schematically. Light pulses for both excitation wavelengths (pulse duration ≈ 5 ns) were generated by tunable dye lasers (Spectra Physics Quanta Ray PDL3), both pumped by the second harmonic of Q-switched, injection seeded Nd:YAG lasers (YAG denotes yttrium aluminum garnet) (Spectra Physics Quanta Ray GCR5 and GCR4). The laser used to generate XUV radiation, required for the B-X transition, was pumped with 700 mJ pulse energy, yielding 160–200 mJ pulse energy at 550 nm using Fluorescein dye. This dye was chosen to obtain the shortest wavelengths that can be generated by a dye pumped with powerful second harmonic radiation from the Nd:YAG laser; this combines the advantages of exciting high vibrational B levels, having a good Franck-Condon overlap close to the minimum in the $\overline{H}$ potential, with high XUV intensity. The visible light was frequency doubled in a KD*P (deuterated KD_2PO_4) crystal, generating UV light with a pulse energy of 40–50 mJ. The UV was separated from the visible by dichroic mirrors and focused into a pulsed gas jet of Xe, creating XUV radiation in the third harmonic at $\lambda\approx 91$ nm. The XUV then propagated into another (differentially pumped) vacuum chamber intersecting at right angles a pulsed hydrogen beam for Doppler-free excitation of the molecules.

The XUV laser was tuned on resonance with a selected rovibronic B-X transition and kept fixed. Resonances were detected through the efficient XUV+UV photoionization that occurs in the presence of the strong UV background from the XUV generation process; ions were extracted with a delayed pulsed electric field and detected with an electron multiplier, discriminating between molecular and atomic ions using their time of flight, as described previously [32–34]. However, for background-free excitation of $\overline{H}$ levels the XUV light must be separated from the UV. This was achieved with a noncollinear phase matching setup described in Ref. [32]. Briefly, a small rod with a diameter of 1 mm

TABLE III. $B''\overline{B}$-$H\overline{H}$ nonrelativistic term values for the lowest 42 vibrational levels in HD. States with dominant $B''\overline{B}$ character are labeled B (inner-well states) or $\overline{B}$ (outer-well states), states with dominant $H\overline{H}$ character are labeled H and $\overline{H}$, respectively; the number following these labels counts the v levels of each subsystem separately.

v	$J=0$	$J=1$	$J=2$	$J=3$	$J=4$	$J=5$
0	113 110.82H0	113 155.88H0	113 245.74H0	113 379.86H0	113 557.43H0	113 777.43H0
1	115 066.93H1	115 109.92H1	115 195.64H1	115 323.58H1	115 492.97H1	115 702.84H1
2	116 928.41H2	116 969.34H2	117 050.95H2	117 172.68H2	117 333.74H2	117 533.05H2
3	117 029.82B0	117 072.06B0	117 156.27B0	117 281.93B0	117 448.30B0	117 654.36B0
4	118 625.05H3	118 661.79H3	118 734.87H3	118 843.52H3	118 986.59H3	119 162.58H3
5	118 839.01B1	118 879.12B1	118 959.10B1	119 078.44B1	119 236.41B1	119 432.05B1
6	119 987.27H4	120 020.06H4	120 085.50H4	120 183.34H4	120 313.27H4	120 474.91H4
7	120 543.90B2	120 581.91B2	120 657.68B2	120 770.73B2	120 920.35B2	121 105.60B2
8	121 355.82H5	121 388.80H5	121 454.49H5	121 552.35H5	121 681.54H5	121 840.90H5
9	122 143.39B3	122 179.27B3	122 250.80B3	122 357.50B3	122 498.67B3	122 673.40B3
10	122 630.24H6	122 660.13H6	122 719.75H6	122 808.79H6	122 926.80H6	123 073.25H6
11	123 074.84$\overline{B}$0	123 076.29$\overline{B}$0	123 079.19$\overline{B}$0	123 083.54$\overline{B}$0	123 089.34$\overline{B}$0	123 096.58$\overline{B}$0
12	123 159.77$\overline{H}$0	123 161.20$\overline{H}$0	123 164.06$\overline{H}$0	123 168.34$\overline{H}$0	123 174.06$\overline{H}$0	123 181.19$\overline{H}$0
13	123 380.17$\overline{B}$1	123 381.63$\overline{B}$1	123 384.54$\overline{B}$1	123 388.91$\overline{B}$1	123 394.73$\overline{B}$1	123 402.01$\overline{B}$1
14	123 464.74$\overline{H}$1	123 466.18$\overline{H}$1	123 469.05$\overline{H}$1	123 473.36$\overline{H}$1	123 479.10$\overline{H}$1	123 486.28$\overline{H}$1
15	123 634.63B4	123 668.33B4	123 683.45$\overline{B}$2	123 687.83$\overline{B}$2	123 693.67$\overline{B}$2	123 700.96$\overline{B}$2
16	123 679.07$\overline{B}$2	123 680.53$\overline{B}$2	123 735.51B4	123 771.09$\overline{H}$2	123 776.86$\overline{H}$2	123 784.06$\overline{H}$2
17	123 762.43$\overline{H}$2	123 763.88$\overline{H}$2	123 766.76$\overline{H}$2	123 835.68B4	123 968.18B4	123 993.50$\overline{B}$3
18	123 837.11H7	123 865.53H7	123 922.09H7	123 980.36$\overline{B}$3	123 986.20$\overline{B}$3	124 074.66$\overline{H}$3
19	123 971.59$\overline{B}$3	123 973.06$\overline{B}$3	123 975.98$\overline{B}$3	124 006.26H7	124 067.44$\overline{H}$3	124 132.10B4
20	124 052.98$\overline{H}$3	124 054.43$\overline{H}$3	124 057.32$\overline{H}$3	124 061.66$\overline{H}$3	124 117.23H7	124 253.97H7
21	124 257.81$\overline{B}$4	124 259.27$\overline{B}$4	124 262.19$\overline{B}$4	124 266.57$\overline{B}$4	124 272.41$\overline{B}$4	124 279.71$\overline{B}$4
22	124 336.50$\overline{H}$4	124 337.95$\overline{H}$4	124 340.85$\overline{H}$4	124 345.19$\overline{H}$4	124 350.99$\overline{H}$4	124 358.22$\overline{H}$4
23	124 537.79$\overline{B}$5	124 539.25$\overline{B}$5	124 542.17$\overline{B}$5	124 546.54$\overline{B}$5	124 552.38$\overline{B}$5	124 559.66$\overline{B}$5
24	124 613.13$\overline{H}$5	124 614.58$\overline{H}$5	124 617.48$\overline{H}$5	124 621.83$\overline{H}$5	124 627.63$\overline{H}$5	124 634.88$\overline{H}$5
25	124 811.64$\overline{B}$6	124 813.09$\overline{B}$6	124 816.00$\overline{B}$6	124 820.37$\overline{B}$6	124 826.18$\overline{B}$6	124 833.45$\overline{B}$6
26	124 883.00$\overline{H}$6	124 884.45$\overline{H}$6	124 887.35$\overline{H}$6	124 891.71$\overline{H}$6	124 897.51$\overline{H}$6	124 904.76$\overline{H}$6
27	124 924.87H8	124 951.19H8	125 003.6H8	125 081.88H8	125 093.93$\overline{B}$7	125 101.17$\overline{B}$7
28	125 013.89B5	125 045.34B5	125 083.78$\overline{B}$7	125 088.13$\overline{B}$7	125 160.76$\overline{H}$7	125 168.01$\overline{H}$7
29	125 079.43$\overline{B}$7	125 080.88$\overline{B}$7	125 108.01B5	125 154.96$\overline{H}$7	125 185.30H8	125 313.11H8
30	125 146.24$\overline{H}$7	125 147.70$\overline{H}$7	125 150.60$\overline{H}$7	125 201.44B5	125 324.97B5	125 362.92$\overline{B}$8
31	125 341.27$\overline{B}$8	125 342.71$\overline{B}$8	125 345.60$\overline{B}$8	125 349.93$\overline{B}$8	125 355.71$\overline{B}$8	125 424.78$\overline{H}$8
32	125 403.00$\overline{H}$8	125 404.45$\overline{H}$8	125 407.36$\overline{H}$8	125 411.72$\overline{H}$8	125 417.53$\overline{H}$8	125 477.70B5
33	125 597.22$\overline{B}$9	125 598.66$\overline{B}$9	125 601.54$\overline{B}$9	125 605.85$\overline{B}$9	125 611.60$\overline{B}$9	125 618.78$\overline{B}$9
34	125 653.41$\overline{H}$9	125 654.87$\overline{H}$9	125 657.77$\overline{H}$9	125 662.13$\overline{H}$9	125 667.94$\overline{H}$9	125 675.20$\overline{H}$9
35	125 847.35$\overline{B}$10	125 848.79$\overline{B}$10	125 851.65$\overline{B}$10	125 855.94$\overline{B}$10	125 861.66$\overline{B}$10	125 868.81$\overline{B}$10
36	125 897.62$\overline{H}$10	125 899.08$\overline{H}$10	125 901.99$\overline{H}$10	125 906.35$\overline{H}$10	125 912.16$\overline{H}$10	125 919.42$\overline{H}$10
37	125 921.24H9	125 944.86H9	125 991.89H9	126 061.93H9	126 105.93$\overline{B}$11	126 113.04$\overline{B}$11
38	126 091.68$\overline{B}$11	126 093.11$\overline{B}$11	126 095.96$\overline{B}$11	126 100.23$\overline{B}$11	126 150.37$\overline{H}$11	126 157.63$\overline{H}$11
39	126 135.82$\overline{H}$11	126 137.27$\overline{H}$11	126 140.18$\overline{H}$11	126 144.55$\overline{H}$11	126 154.42H9	126 268.61H9
40	126 277.62B6	126 306.77B6	126 334.39$\overline{B}$12	126 338.65$\overline{B}$12	126 344.33$\overline{B}$12	126 351.42$\overline{B}$12
41	126 330.12$\overline{B}$12	126 331.55$\overline{B}$12	126 364.86B6	126 376.97$\overline{H}$12	126 382.79$\overline{H}$12	126 390.06$\overline{H}$12

was placed in the center of the incident UV beam, thus creating a shadow in the far field behind the focus inside the vacuum chamber. A slit was inserted to efficiently block the UV, but not the XUV, which is generated closer to the optical axis.

The second laser pulse was counterpropagated through the interaction vacuum chamber, overlapping with the XUV and the probe gas beam. Temporal overlap with the XUV pulse is required, imposed by the short lifetime of the B state (≈ 1 ns); it was achieved by external control of the triggers

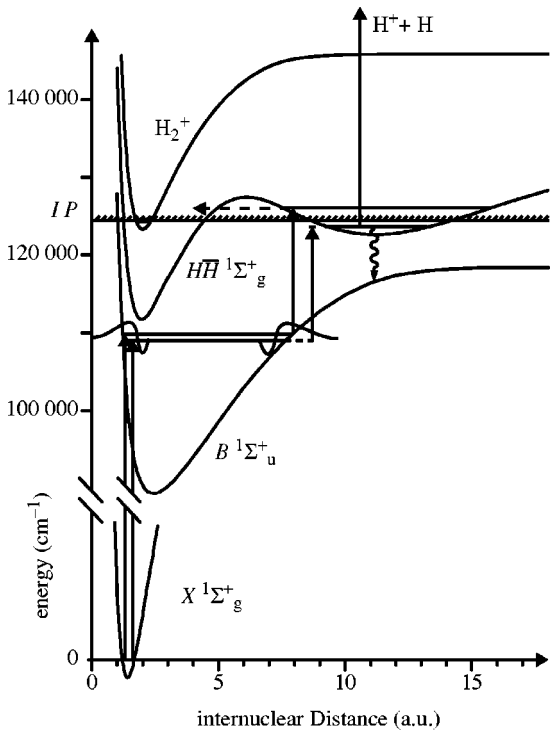

FIG. 2. Excitation scheme for H_2 and D_2, showing the two-photon excitation of the $\overline{H}\,^1\Sigma_g^+$ state from the $X\,^1\Sigma_g^+$ ground state via the intermediate $B\,^1\Sigma_u^+$ state. In the case of HD, this scheme is also used to excite the $\overline{B}\,^1\Sigma_u^+$ state; in the symmetric isotopomers this transition is dipole forbidden.

of the Q switches of both Nd:YAG lasers (Stanford Research Systems DG535 delay/pulse generator). Several dyes were used to cover a wide wavelength range (556–735 nm): Rhodamine-6G, Rhodamine-B, a mixture of these two dyes, DCM, and Styryl-8. Molecules in excited states were probed by ionization with a 355 nm laser pulse (≈ 20 mJ) from the third harmonic of one of the Nd:YAG lasers, delayed by 20 ns with an optical delay line. Ions were again extracted by a pulsed field of 100 V/cm and detected separately (by time of flight) for different mass.

A large wavelength range was first explored to find the $\overline{H}$ excitations by tuning the second laser in large steps of 0.1 cm^{-1} per pulse, running at full power (2–5 mJ) to obtain strong signals. The upper trace of Fig. 4 shows an example of such a spectrum, recorded with the XUV laser fixed to the B-$X(19,0)R(0)$ transition while scanning the second laser over the range 600–670 nm. Transitions to various vibrational $\overline{H}$ levels in H_2 were observed on a noisy background of broad resonances, with the $R(1)$ and $P(1)$ transitions from each band leading to upper levels with $J=0$ and 2. For accurate measurements the pulse energy of the second laser was reduced until peak signal height decreased linearly with intensity, thus avoiding saturation broadening; depending on transition strength (and also on the transverse profile of the laser beam) between 1 mJ/pulse and 4 μJ/pulse was required. The laser was then scanned in steps of 0.01 cm^{-1}, averaging over four or eight pulses to increase the signal/noise ratio.

The wavelength of the second laser was calibrated using a simultaneously recorded transmission spectrum of an I_2 cell

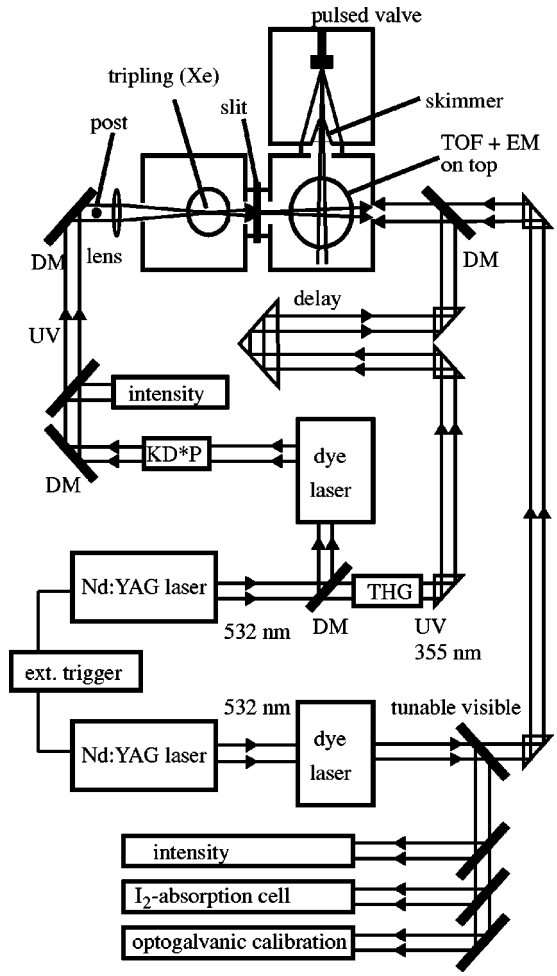

FIG. 3. Schematic of the experimental setup. Essential parts of the laser system, generating nanosecond light pulses at three different wavelengths, are shown. Frequency tripling of the first laser pulse and excitation of hydrogen molecules are performed in two interconnected and differentially pumped vacuum chambers. A central trigger system synchronizes the light pulses and the pulsed field for extraction of ions, the mass-separated detection, and on-line signal registration. TOF: time of flight; EM: electron multiplier; DM: dichroic mirror; THG: third harmonic generation crystal for Nd:YAG.

(length ≈ 40 cm). Only a small fraction of the laser light was passed through the cell to avoid saturation broadening of the I_2 transitions. A satisfactory absorption spectrum is obtained when peak absorption is between 10% and 50%. To achieve this the absorption cell was used single pass at room temperature for wavelengths <600 nm and with a fivefold pass for $\lambda > 600$ nm. At $630 < \lambda < 675$ nm the cell was heated to $\approx 60\,°C$ to increase thermal population of absorbing levels. An example of a $\overline{H}$-B spectrum of D_2 with I_2 calibration is shown in Fig. 5. Frequencies of absorption lines that are clearly resolved were assigned with wave numbers taken from Ref. [35], marked with an asterisk in the I_2 spectrum. The frequency scale was then determined by a spline through the assigned absorption lines. Multiple scans of the same transitions as well as different choices of calibration lines reproduce line positions within 0.02 cm^{-1} (1σ). Longer wavelengths were calibrated optogalvanically with a hollow cathode discharge in argon,

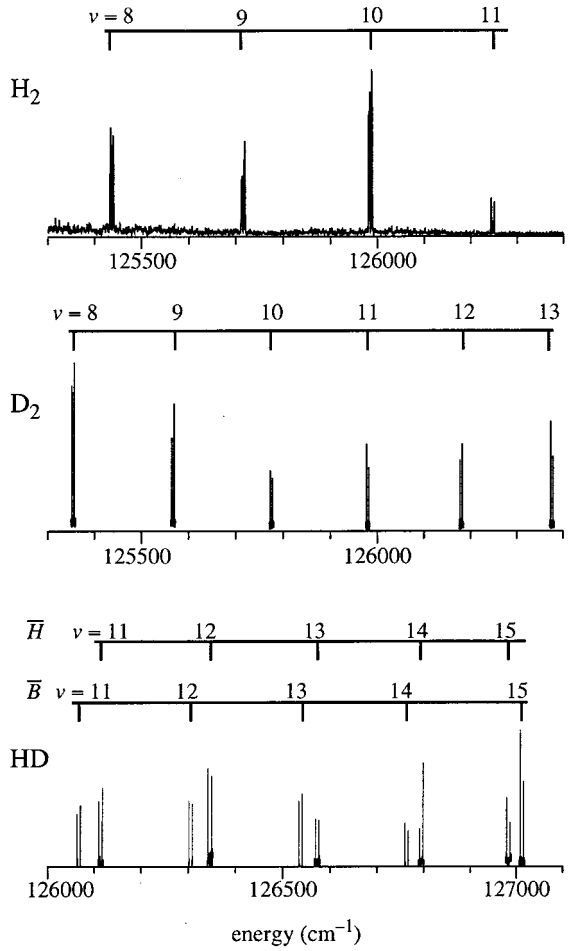

FIG. 4. Overview spectra of excitation of several vibrational $\overline{H}$ levels in H_2 and D_2, and $\overline{H}$ and $\overline{B}$ levels in HD. In H_2 the spectrum is recorded in a long scan of the second laser with a fixed intermediate state, while in D_2 and HD short scans around the level energies were put together. In all cases, each vibrational band consists of a doublet belonging to a $P(\Delta J=-1)$ and $R(\Delta J=+1)$ rotational transition.

wave numbers taken from Ref. [36], where the accuracy is limited by line shape and linewidth effects of the optogalvanic signal to about 0.1 cm^{-1}.

IV. SPECTROSCOPIC RESULTS

In Fig. 4 overview spectra of the $\overline{H}$ state for the investigated isotopomers are shown. The upper trace was recorded in a single overview scan in H_2, while the lower traces (D_2 and HD) are composed of several short scans. We observed

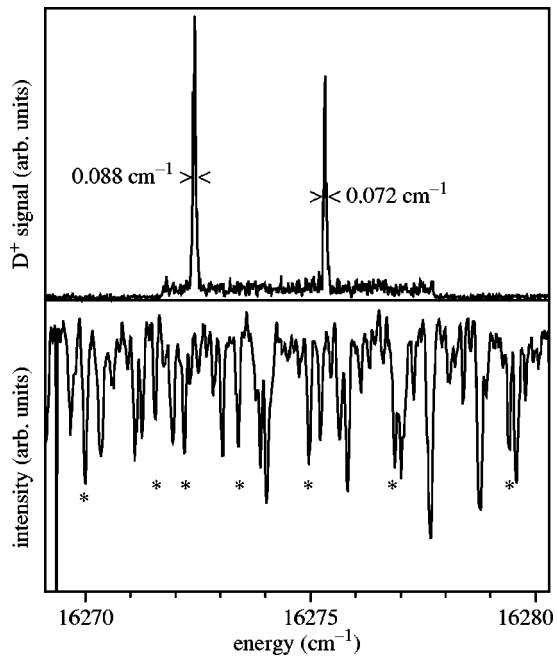

FIG. 5. Spectrum of the $R(1)$, and $P(1)$ transitions of the $\overline{H}$-B (9,25) band in D_2 with an I_2 transmission spectrum recorded simultaneously; lines marked by an asterisk are used for calibration.

vibrational $\overline{H}$ levels with $v=2$–15, $J=0$–5 in H_2; $v=6$–22, $J=0$–5 in D_2; $v=4$–17, $J=0$–3 in HD; and in HD also $\overline{B}$ levels with $v=9$–20, $J=0$–3. Observation of low vibrational $\overline{H}$ levels is restricted by their Franck-Condon factors with the highest v levels of the intermediate B state used; overlap then only exists for the tail of the vibrational wave functions in the classically forbidden region.

To determine total energies, measured transition energies were added to the energies of rovibronic $B\,^1\Sigma_u^+$ energies; in many cases several intermediate levels were used to populate the same excited states for a check of combination differences. B level energies were determined by adding rotational energies of the $X\,^1\Sigma_g^+$ ground state level, taken from Ref. [37] for H_2, from Ref. [38] for HD, and from Ref. [39] for D_2, to the B-X transition energy. In the case of H_2 we used B, $v=18$ and 19, $J=0$–4 as intermediate states, taking directly the values for transition wave numbers from Ref. [33] with the exception of the $v=18$, $J=4$ level, which had to be lowered by 0.16 cm^{-1} to 108 491.51 cm^{-1} after checking combination differences for $J=3$ excited levels.

In D_2 we used B, $v=25$–27, $J=1$–4 as intermediate levels. Level energies were again taken from Ref. [33], but some levels were missing and some others had rather large uncertainties. Therefore we applied an additional correction

TABLE IV. Energies of B levels in D_2 used as intermediates, corrected by a combination difference analysis. Δ refers to their deviations from Ref. [33]. All values in cm^{-1}.

	$J=1$		$J=2$		$J=3$		$J=4$	
v	E	Δ	E	Δ	E	Δ	E	Δ
25	109 291.61	−0.07	109 312.00	−0.02	109 342.59	0.00	109 838.24	0.00
26	109 847.52	0.00	109 867.80	+0.02	109 898.46	−0.05	109 940.20	[a]
27	110 390.06	+0.05	110 409.50	[a]	110 438.71	0.00	110 477.47	+0.04

[a]Level not observed in Ref. [33].

TABLE V. Experimental energies of B and EF levels in HD used as intermediates. Δ refers to deviations from Ref. [26]. All values in cm^{-1}.

	$J=1$		$J=2$	
State	E	Δ	E	Δ
$B(21)$	109 406.07	-0.11 [a]	109 435.74	$+0.39$
$B(22)$	110 071.35	$+0.32$	110 101.41	$+0.34$
$B(23)$	110 715.16	$+0.39$	110 743.35	$+0.54$
$EF(19)$	110 750.53	$+0.31$	110 781.75	$+0.28$

[a] $+0.36$ if B-X (21,0) $R(0)$ transition is discarded in Ref. [26].

based on combination differences in the second excitation step: each B level was given an offset proportional to its experimental accuracy, minimizing combination differences in the system of $\overline{H}$-B transitions. This procedure was applied separately for levels of para- and ortho-hydrogen, and finally the two classes of levels were shifted against each other with the criterion of obtaining smooth rotational bands in the $\overline{H}$ state. The resulting B rovibronic level energies in D_2 are listed in Table IV. As a result the uncertainty of these values is dominated by the accuracy of the calibration of the visible dye laser (0.02 cm^{-1}) and the uncertainty of the most accurate energies in Ref. [33], 0.03 cm^{-1}. Therefore the resulting uncertainty for each level is ≈ 0.04 cm^{-1}.

In HD the intermediate levels were B, $v=21$–23 and EF, $v=19$, $J=1$ and 2; accurate energies of these states were not available. We determined them scanning the XUV laser over the desired wavelength range using a mixture of H_2, D_2, and HD, recording the XUV+UV photoionization signal. Resonances in HD were calibrated first with the energies of excited levels in H_2 and D_2 taken from Refs. [33,34]; from the discrepancy between a point-to-point frequency scale and a smoothed one we estimate an uncertainty for HD levels of 0.2 cm^{-1}. In a second step combination differences in transitions to $\overline{H}$ and $\overline{B}$ levels were used to correct the energy values in the same way as in D_2. Assuming that the uncertainties for the uncorrected energies are not correlated, we conclude that the systematic deviation for the system of corrected energies is probably smaller than 0.06 cm^{-1}. Table V shows the resulting energies of levels that were used as intermediates. Reference is made to the hitherto most accurate values for their energies [26]. Note that the EF-X transition is dipole allowed in HD due to g-u symmetry breaking; the $EF\,^1\Sigma_g^+$, $v=19$ level is strongly mixed with the near-coincident $B\,^1\Sigma_u^+$, $v=23$ level, resulting in an appreciable transition strength from the ground state.

For measurements on HD the ionization laser pulse at 355 nm was not delayed but temporally overlapped with the other two light pulses, because the excited state decays too rapidly. The result was a poorer signal to background ratio due to direct ionization of the intermediate B or EF state by a 355 nm photon. This process produces mainly HD^+ ions and its yield is strongly correlated with the excitation of $\overline{H}$ levels through fluctuations in the population of the intermediate state; therefore the noise on the background can be strongly reduced by dividing the H^+ (or D^+) and HD^+ signals. When the EF, $v=19$ intermediate state was used, the result was slightly improved by replacing the 355 nm pulse with the fundamental UV pulse (≈ 273 nm) used for the XUV generation. This was achieved by removing the rod and the slit that otherwise performed the wavelength separation; the reason for this difference is, however, unclear.

Tables VI, VII, and VIII contain values for experimental energies of all observed $\overline{H}$ (and $\overline{B}$) rovibronic levels in H_2, D_2, and HD, respectively. For H_2 individual uncertainties are given, depending on the uncertainties of the intermediate B states; $\overline{H}$, $v=9$–11 levels were remeasured to the same level

TABLE VI. Observed $\overline{H}$ level energies in H_2 in cm^{-1} with respect to the ground state, in parentheses the experimental uncertainty in the last digit. Δ_{o-c} refers to values from Ref. [12] (including relativistic corrections). For levels that were not observed, calculated values are given in italics.

	$J=0$		$J=1$		$J=2$		$J=3$		$J=4$		$J=5$	
v	E	Δ_{o-c}	E	Δ_{o-c}	E	Δ_{o-c}	E	Δ_{o-c}	E	Δ_{o-c}	E	Δ_{o-c}
0	*122 883.41*		*122 885.31*		*122 889.12*		*122 894.83*		*122 902.44*		*122 911.95*	
1	*123 234.08*		*123 235.99*		*123 239.82*		*123 245.57*		*123 253.23*		*123 262.79*	
2	123 575.9 (2)	+0.8	123 577.7 (2)	+0.7	123 581.7 (2)	+0.9	123 587.3 (2)	+0.7	123 595.4 (2)	+1.1	123 604.3 (5)	+0.4
3	907.34(6)	+0.79	909.26(3)	+0.78	913.12(6)	+0.78	918.87(3)	+0.75	926.58(3)	+0.75	936.4 (1)	+0.9
4	124 229.63(6)	+0.90	124 231.56(3)	+0.90	124 235.41(3)	+0.88	124 241.21(3)	+0.89	124 248.92(3)	+0.88	124 258.59(5)	+0.90
5	542.75(6)	+0.96	544.69(3)	+0.97	548.55(3)	+0.96	554.38(3)	+0.99	562.07(3)	+0.95	571.75(5)	+0.98
6	846.96(6)	+1.05	848.89(3)	+1.04	852.74(3)	+1.02	858.59(5)	+1.06	866.28(3)	+1.02	875.95(5)	+1.03
7	125 142.37(4)	+1.08	125 144.30(6)	+1.08	125 148.14(6)	+1.04	125 154.02(5)	+1.11	125 161.68(3)	+1.03	125 171.38(5)	+1.07
8	429.15(6)	+1.10	431.13(6)	+1.14	434.95(6)	+1.08	440.79(3)	+1.10	448.50(3)	+1.06	458.20(5)	+1.09
9	707.50(4)	+1.14	709.49(6)	+1.19	713.32(4)	+1.13	719.18(4)	+1.16	726.91(5)	+1.13	736.62(4)	+1.15
10	977.42(3)	+1.13	979.44(4)	+1.19	983.27(3)	+1.12	989.14(4)	+1.14	996.90(5)	+1.11	126 006.62(4)	+1.11
11	126 238.99(3)	+1.08	126 241.05(4)	+1.18	126 244.85(3)	+1.05	126 250.83(4)	+1.15	126 258.59(5)	+1.08	268.37(4)	+1.09
12	492.20(6)	+1.04	494.16(3)	+1.01	498.11(4)	+1.01	504.05(3)	+1.00	511.92(3)	+0.97	521.75(5)	+0.95
13	736.83(6)	+0.99	738.85(3)	+0.99	742.83(3)	+0.94	748.84(5)	+0.92	756.86(3)	+0.93	766.83(5)	+0.91
14	972.39(6)	+0.68	974.44(3)	+0.60	978.50(3)	+0.11	984.80(3)	+1.40	992.80(3)	+0.86	127 003.20(5)	+0.98
15	127 197.46(3)	+0.55	127 199.70(5)	+0.56	127 204.09(3)	+0.50	127 210.64(3)	+0.36	127 219.46			
16	*127 405.68*		*127 408.74*		*127 414.54*		*127 422.74*		*127 433.18*			

TABLE VII. Observed $\overline{H}$ level energies in D_2 in cm^{-1} with respect to the ground state; the experimental uncertainty is 0.04 cm^{-1}. Δ_{o-c} refers to results of a calculation analogous to Ref. [12]. For levels that were not observed, calculated values are given in italics.

	$J=0$		$J=1$		$J=2$		$J=3$		$J=4$		$J=5$	
v	E	Δ_{o-c}	E	Δ_{o-c}	E	Δ_{o-c}	E	Δ_{o-c}	E	Δ_{o-c}	E	Δ_{o-c}
0	*123 482.19*		*123 483.14*		*123 485.04*		*123 487.90*		*123 491.71*		*123 496.46*	
1	*732.42*		*733.38*		*735.29*		*738.16*		*741.99*		*746.77*	
2	*977.76*		*978.72*		*980.64*		*983.52*		*987.36*		*992.16*	
3	*124 218.26*		*124 219.23*		*124 221.15*		*124 224.04*		*124 227.89*		*124 232.70*	
4	*453.99*		*454.96*		*456.89*		*459.78*		*463.64*		*468.46*	
5	*685.03*		*686.00*		*687.93*		*690.83*		*694.69*		*699.52*	
6	124 911.93	+0.50	124 912.82	+0.42	124 914.80	+0.47	124 917.67	+0.45	124 921.56	+0.46	124 926.34	+0.40
7	125 133.71	+0.44	125 134.72	+0.48	125 136.62	+0.44	125 139.55	+0.47	125 143.4	+0.45	125 148.26	+0.47
8	351.09	+0.47	352.08	+0.49	354.02	+0.50	356.93	+0.50	360.81	+0.51	365.63	+0.49
9	564.04	+0.51	565.01	+0.51	566.95	+0.51	569.86	+0.51	573.76	+0.54	578.57	+0.50
10	772.59	+0.51	773.54	+0.49	775.51	+0.52	778.37	+0.47	782.31	+0.53	787.12	+0.50
11	976.83	+0.51	977.78	+0.49	979.73	+0.50	982.62	+0.51	986.54	+0.52	991.37	+0.50
12	126 176.82	+0.53	126 177.76	+0.49	126 179.74	+0.53	126 182.59	+0.46	126 186.51	+0.50	126 191.38	+0.52
13	372.58	+0.53	373.50	+0.48	375.51	+0.54	378.39	+0.50	382.30	+0.52	387.17	+0.53
14	564.13	+0.51	565.08	+0.48	567.05	+0.50	569.97	+0.49	573.86	+0.48	578.73	+0.48
15	751.55	+0.52	752.48	+0.47	754.49	+0.52	757.38	+0.47	761.31	+0.49	766.16	+0.45
16	934.76	+0.48	935.75	+0.49	937.71	+0.48	940.62	+0.44	944.58	+0.47	949.47	+0.45
17	127 113.82	+0.48	127 114.76	+0.43	127 116.76	+0.45	127 119.73	+0.45	127 123.69	+0.45	127 128.62	+0.44
18	288.63	+0.46	289.59	+0.42	291.62	+0.45	294.59	+0.43	298.59	+0.44	303.54	+0.41
19	459.06	+0.42	460.05	+0.40	462.10	+0.42	465.09	+0.38	469.16	+0.41	474.17	+0.38
20	624.91	+0.36	625.90	+0.31	628.01	+0.35	631.06	+0.23	635.20	+0.41	640.27	+0.33
21	785.68	+0.28	786.69	+0.23	788.90	+0.31	792.05	+0.27	796.22	+0.20	801.48	+0.14
22	940.10 [a]	+0.38	941.32	+0.42	*127 943.24*		945.11	+0.42	951.28	+0.04	957.17	+0.31

[a]Broadened and overlapping with $J=2$.

of accuracy as for the other vibrational levels; in Ref. [22] calibration problems caused a larger uncertainty. For D_2 and HD the correction procedure leads to a common statistical uncertainty of 0.04 cm^{-1} for all levels, with an additional systematic uncertainty of 0.06 cm^{-1} in HD as explained above.

For high vibrational levels in the $\overline{H}$ state, and also in the $\overline{B}$ state in HD, the lines are strongly broadened. In Fig. 6 an example is shown of the $\overline{H}$, $v=22$, $J=0$, and $J=2$ levels in D_2, excited from the B, $v=27$, $J=1$ intermediate level; rotational levels are no longer resolved. Although the uncertainty in the peak position is still determined by the accuracy of the calibration, the error in the experimental level energy is probably larger; especially in cases where broadened lines are asymmetric. This broadening indicates a shortened lifetime due to a quick decay process that involves tunneling through the top of the barrier in the $H\overline{H}\,^1\Sigma_g^+$ potential. The intramolecular dynamics of tunneling and subsequent autoionization and dissociation, which is particularly complicated in the HD isotopomer, will be the subject of a future paper.

V. DISCUSSION

A. The $\overline{H}$ state in H_2 and D_2

Experimental $\overline{H}$ rovibronic level energies in H_2 can be compared with *ab initio* values from Ref. [12], now presented in more detail; note that experimental results have slightly changed for $v=9$–11 with respect to Ref. [22]. Energies in D_2 are calculated in the same way as for H_2 [12,24]. The calculation of adiabatic vibrational wave functions naturally treats levels in the entire potential in a unified way without explicitly discriminating between outer-well and inner-well states. At energies far below the intermediate barrier, wave function amplitude always concentrates in either well, as long as there are no accidental coincidences; even in that case level shifts are small [17].

Calculated energies are slightly lower than experimental values by about 1 cm^{-1} in H_2 and 0.5 cm^{-1} in D_2 over a wide range of vibrational quantum numbers. Variation with v shows the same pattern in both isotopes: in H_2 the discrepancy first increases from 0.75 cm^{-1} ($v=3$) to 1.15 cm^{-1} ($v=9$) and then decreases again to 0.95 cm^{-1} ($v=13$); we average over the six observed rotational levels for each v. The highest observed levels show considerable scatter, ranging from 0.11 cm^{-1} ($v=14$, $J=2$) to 1.40 cm^{-1} ($v=14$, $J=3$). In D_2 the deviation slightly increases from 0.45 cm^{-1} ($v=6$) to 0.52 cm^{-1} ($v=13$) and then decreases to 0.24 cm^{-1} ($v=21$), again with increasing scatter between J levels. The maximum of the deviation occurs at the same binding energy for both isotopes; this is not directly reflected by the level energies as given in the tables, because they are defined relative to the ground states of H_2 and D_2, which have different zero-point vibrational energy. The ratio of the deviations in H_2 and D_2 matches approximately their reduced mass ratio, which is consistent with an assumption made previously [12,24] that deviations are due to nonadiabatic interactions. The sign of

TABLE VIII. Observed $\overline{H}$ and $\overline{B}$ level energies in HD in cm^{-1} with respect to the ground state; states of mixed character are assigned according to the major contribution. Systematic experimental uncertainty 0.06 cm^{-1}; individual uncertainty of each level 0.04 cm^{-1} unless a different value is given.

		$J=0$		$J=1$		$J=2$		$J=3$	
	v	E	Δ_{o-c}	E	Δ_{o-c}	E	Δ_{o-c}	E	Δ_{o-c}
$\overline{H}$	4	124 337.17	+0.67	124 338.63	+0.68	124 341.51	+0.66	124 345.88	+0.69
$\overline{H}$	5	613.84	+0.71	615.29	+0.71	618.20	+0.72	622.59	+0.76
$\overline{H}$	6	883.73	+0.73	884.57	+0.12	888.09	+0.74	892.03	+0.32
$\overline{H}$	7	125 147.00	+0.76	125 148.46	+0.76	125 151.37	+0.77	125 155.71	+0.75
$\overline{H}$	8	403.76	+0.76	405.17	+0.72	408.12	+0.76	412.42	+0.70
$\overline{B}$	9			599.84	+1.18			607.03	+1.18
$\overline{H}$	9	654.24	+0.83	655.55	+0.68	658.49	+0.72	662.82	+0.69
$\overline{B}$	10	848.64	+1.29	850.13	+1.34	852.94	+1.29	857.20	+1.26
$\overline{H}$	10	898.31	+0.69	899.71	+0.63	902.68	+0.69	906.97	+0.62
$\overline{B}$	11	126 093.04	+1.36	126 094.45	+1.34	126 097.33	+1.37	126 101.57	+1.34
$\overline{H}$	11	136.39	+0.57	137.82	+0.55	140.78	+0.60	145.08	+0.53
$\overline{B}$	12	331.58	+1.46	332.98	+1.43	335.74	+1.35	340.09	+1.44
$\overline{H}$	12	368.69	+0.46	370.12	+0.43	373.08	+0.48	377.40	+0.43
$\overline{B}$	13	563.96	+1.55	565.35	+1.51	568.23	+1.55	572.45	+1.51
$\overline{H}$	13	595.63	+0.35	597.01	+0.27	599.99	+0.34	604.28	+0.27
$\overline{B}$	14	789.53	+1.60	790.95	+1.58	793.83	+1.60	798.12	+1.60
$\overline{H}$	14	817.87	+0.21	819.27	+0.26	822.21	+0.21	826.48	+0.14
$\overline{H}$	15	127 007.27	+1.54	127 008.70	+1.51	127 011.65	+1.54	127 015.98	+1.50
$\overline{B}$	15	036.48	+0.19	037.88	+0.16	040.76	+0.18	045.02	+0.15
$\overline{H}$	16	216.43	+1.34	217.88	+1.29	220.93	+1.34	225.40	+1.32
$\overline{B}$	16	252.00	+0.29	253.38	+0.26	256.24	+0.31	260.71	+0.56
$\overline{H}$	17	416.93	+1.56	417.89	+0.90	421.56	+1.37	425.80	+0.88
$\overline{B}$	17	464.00	+0.48	465.41	+0.47	468.17	+0.42	472.36	+0.43
$\overline{H}$	18	607.76	−1.43	609.66	−1.71	613.70	−2.94	616.7	+10.6[a]
$\overline{B}$	18	672.05	+0.36	673.44	+0.35	676.29	+0.38	680.45	+0.18
$\overline{H}$	19	781.3[b]	−6.4	789.24	−0.73	791.3[b]	−3.2	797.4[b]	−4.0
$\overline{B}$	19	875.47	+0.81	876.66	+0.55	880.15	+1.17	882.72	−0.53
$\overline{B}$	20	128 075.8[b]	−5.8	128 079.3[b]	−5.1	128 082.7[b]	−8.7	128 085.8[b]	+8.1

[a]Identification ambiguous; two calculated levels at 127 606.12 and 127 635.08 cm^{-1} are both not clearly localized in one potential well.
[b]Experimental uncertainty 0.3 cm^{-1}.

the shift indicates that the interaction with lower-lying states should be dominant, i.e., with the EF and $GK\,^1\Sigma_g^+$ states.

Vibrational levels close to the $H\overline{H}$ potential barrier show a slightly perturbed rotational structure, i.e., some deviations occur from a fit of the energies of rotational levels for each vibrational state to the rigid rotator formula $E(J)=T_v+B_vJ(J+1)$; higher terms in $J(J+1)$ do not differ from zero significantly for any v. Molecular constants for H_2 were previously reported [22], values for D_2 are given in Table IX. The small deviations near the top of the barrier can be explained by the increasing influence of the spreading of the vibrational wave function over both potential wells. This is automatically accounted for in the calculation of adiabatic rovibrational energies, which treats the entire potential as a whole. The centrifugal potential is included for each rotational quantum number, resulting for each J in a different order of levels with wave functions concentrated in either of the two potential wells.

For the perturbed rotational structure of the experimentally determined level energies we therefore expect the usual pattern of avoided crossings at the J values where an inner- and an outer-well vibrational state change their order on the energy scale. Although only few deviations are significant with respect to experimental uncertainty, the avoided-crossing pattern is found unambiguously in the $v=14$ level in H_2: the $J=3$ level is shifted upwards and the $J=4$ level downwards by 0.1 cm^{-1}, which is consistent with a perturbing state at small internuclear distance. However, the calculation predicts the crossing point to lie between $J=2$ and 3; the $J=3$ inner-well state must lie at least 50 cm^{-1} lower than calculated to be consistent with the observed level ordering. A qualitative explanation can be given by assuming

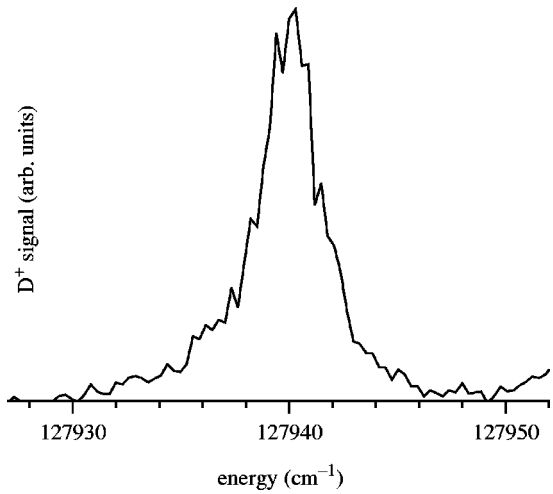

FIG. 6. Broadened $\overline{H}$ level ($v=22$ in D_2) close to the barrier in the $H\overline{H}$ potential, indicating efficient tunneling through the barrier followed by fast decay. The $J=0$ and 2 states are not resolved.

that nonadiabatic interactions with other electronic states play a major role for the levels at small internuclear distance. At lower energies this is an established fact, and calculations show that level shifts of tens of cm^{-1} occur, in agreement with experiment; the adiabatic approximation breaks down completely, and energy levels must be described by superpositions of many adiabatic wave functions, which are different for each J [10]. It is therefore an oversimplification to consider the perturbing states as adiabatic $H\,^1\Sigma_g^+$ inner-well states with well-behaved rotational structure; what is remarkable is the small deviation of outer-well level energies from the adiabatic values.

B. The $\overline{H}$ and $\overline{B}$ states in HD

Experimental energies of most observed $\overline{H}$ and $\overline{B}$ states in HD agree with calculated values within 1.5 cm^{-1} (see Table VIII), except for the highest ones. Electronic labels are only indicative, for all observed levels are superpositions of $H\overline{H}\,^1\Sigma_g^+$ and $B''\overline{B}\,^1\Sigma_u^+$ wave functions, as discussed in Ref. [28]. The present calculation confirms that the labels correspond indeed to the electronic contributions with the largest coefficient. Vibrational levels are counted separately for outer-well $\overline{H}$ and $\overline{B}$ states as in Ref. [28]; these numbers are included in Table III. The calculation also confirms the absolute v values, which could not be derived from experiment because the lowest vibrational levels were not observed. The strongest mixing of g and u wave function character is found for the $\overline{H}$, $v=14$ and $\overline{B}$, $v=14$ states, having a component of the opposite symmetry of more than 40% each, for $J=0$–3, in agreement with the earlier semiempirical analysis [28].

Deviations between observed and calculated energies in HD show a slightly more complicated pattern than in the homonuclear isotopomers; but with few exceptions, they vary smoothly with v and J. The lowest observed vibrational $\overline{H}$ levels, $v=4$–10, which have only small $\overline{B}$ admixture, lie ≈ 0.7 cm^{-1} higher than calculated. When scaled with the reduced mass for HD this is consistent with the supposed source of deviations in H_2 and D_2, the neglected nonadiabatic interactions with other states with gerade symmetry. The deviations for observed $\overline{B}$ levels in the same energy region are clearly different from those for $\overline{H}$ (≈ 1.2–1.3 cm^{-1}), which is not surprising because of different nonadiabatic couplings with other states. In the region of $12 \leqslant v \leqslant 17$, where strong g-u mixing occurs, the interpretation is less straightforward. Here we find close-lying pairs of an $\overline{H}$ and a $\overline{B}$ state, with equal J and, coincidentally, equal v quantum numbers. Between $v=14$ and $v=15$, for each J the upper state of such a pair formally changes its label from $\overline{H}$ to $\overline{B}$ (and the lower state vice versa), but the change between g and u electronic character is actually smooth; therefore the change of deviations for the upper and lower states of a pair rather than for $\overline{H}$ and $\overline{B}$ has to be followed. One finds (cf. Table VIII) that the difference between observed and calculated energies goes through a minimum for the upper and through a maximum for the lower levels at the point of maximal interaction; this suggests that the g-u interaction between $\overline{H}$ and $\overline{B}$ states is slightly weaker than calculated. For the highest $\overline{H}$ levels close to the internal potential barrier, whose vibrational wave functions stretch over both wells, the deviation quickly changes; a correct prediction of the energies would require that nonadiabatic interactions with other electronic states of both g and u symmetry are included. The same holds for the highest $\overline{B}$ levels, which lie higher than the barrier of the $H\overline{H}$ potential.

TABLE IX. Fit parameters of a rigid-rotor fit to experimental level energies in D_2.

v	$T_v(cm^{-1})$[a]	$B_v(cm^{-1})$[b]
6	124 911.90	0.4817
7	125 133.73	0.4845
8	125 351.11	0.4845
9	125 564.04	0.4847
10	125 772.58	0.4849
11	125 976.82	0.4852
12	126 176.80	0.4855
13	126 372.56	0.4869
14	126 564.12	0.4870
15	126 751.54	0.4877
16	126 934.76	0.4903
17	127 113.80	0.4942
18	127 288.62	0.4974
19	127 459.06	0.5041
20	127 624.91	0.5129
21	127 785.69	0.5269

[a]Uncertainty 0.01 cm^{-1}.
[b]Uncertainty 0.002 cm^{-1}.

VI. CONCLUSION

The energy level structure of the outer-well part of the highly excited $H\overline{H}\,^1\Sigma_g^+$ double-well potential in molecular hydrogen was experimentally determined via multistep laser excitation and compared with accurate *ab initio* calculations. For the inversion symmetric species H_2 and D_2 the outer-well states can be considered in very good approximation as

levels of an isolated rigid-rotor molecular system. *Ab initio* predictions including relativistic effects produce agreement within 0.5 cm^{-1} for D_2 and within 1.0 cm^{-1} for H_2. In HD the inversion symmetry of the $\bar{H}\,^1\Sigma_g^+$ outer-well state is strongly broken. This phenomenon is analyzed in terms of a nonadiabatic interaction between the $\bar{H}\,^1\Sigma_g^+$ state and the $\bar{B}\,^1\Sigma_u^+$ outer-well state, which has a similar atomic-orbital configuration. Inclusion of this *g*-*u* interaction in the *ab initio* calculations leads to an agreement with experiment within 1.5 cm^{-1}.

The $H\bar{H}\,^1\Sigma_g^+$ state is one of a series of exotic double-well states with nearly pure ionic character at large internuclear distance, correlating with a neutral-atom dissociation channel; in the case of $\bar{H}$ beyond 36 a.u. the potential curve levels off to the $(n=1)+(n=3)$ limit. Similar long range states are predicted below the $n=4$ and $n=5$ limits for both *g* and *u* symmetries [40]. For the $n=4$ case isolated outer-well states should exist at >1 eV above the ionization limit of the molecule, with vibrational wave functions bound between ≈ 15 and 80 a.u. The excitation of these exotic states will be the subject of future investigations.

ACKNOWLEDGMENTS

This work was supported in part by a Polish KBN Grant No. 2 P03B 022 12 to L. Wolniewicz, and by a USF grant from Vrije Universiteit.

[1] L. Wolniewicz, J. Chem. Phys. **78**, 6173 (1983).
[2] L. Wolniewicz, J. Chem. Phys. **103**, 1792 (1995).
[3] A. Balakrishnan, V. Smith, and B. P. Stoicheff, Phys. Rev. Lett. **68**, 2149 (1992).
[4] A. Balakrishnan and B. P. Stoicheff, J. Mol. Spectrosc. **156**, 517 (1992).
[5] E. F. McCormack and E. E. Eyler, Phys. Rev. Lett. **66**, 1042 (1991).
[6] E. E. Eyler and N. Melikechi, Phys. Rev. A **48**, R18 (1993).
[7] J. M. Gilligan and E. E. Eyler, Phys. Rev. A **46**, 3676 (1992).
[8] D. Shiner, J. M. Gilligan, B. M. Cook, and W. Lichten, Phys. Rev. A **47**, 4042 (1993).
[9] P. Quadrelli, K. Dressler, and L. Wolniewicz, J. Chem. Phys. **93**, 4958 (1990).
[10] S. Yu and K. Dressler, J. Chem. Phys. **101**, 7692 (1994).
[11] L. Wolniewicz, J. Chem. Phys. **105**, 10 691 (1996).
[12] L. Wolniewicz, J. Chem. Phys. **109**, 2254 (1998).
[13] S. C. Ross and Ch. Jungen, Phys. Rev. A **49**, 4353 (1994).
[14] E. R. Davidson, J. Chem. Phys. **33**, 1577 (1960).
[15] E. E. Marinero, R. Vasudev, and R. N. Zare, J. Chem. Phys. **78**, 692 (1983).
[16] P. Senn, P. Quadrelli, K. Dressler, and G. Herzberg, J. Chem. Phys. **83**, 962 (1985).
[17] P. Senn and K. Dressler, J. Chem. Phys. **87**, 1205 (1987).
[18] K. Dressler, R. Galluser, P. Quadrelli, and L. Wolniewicz, J. Mol. Spectrosc. **759**, 205 (1979).
[19] L. Wolniewicz and K. Dressler, J. Mol. Spectrosc. **77**, 286 (1979).
[20] J. Ishi, K. Tsukiyama, and K. Uehara, Laser Chem. **14**, 31 (1994).
[21] H. Suzuki, M. Nakata, Y. Ogi, and K. Tsukiyama, J. Mol. Spectrosc. **191**, 142 (1998).
[22] E. Reinhold, W. Hogervorst, and W. Ubachs, Phys. Rev. Lett. **78**, 2543 (1997).
[23] L. Wolniewicz and K. Dressler, J. Chem. Phys. **82**, 3292 (1985).
[24] L. Wolniewicz, J. Chem. Phys. **108**, 1499 (1998).
[25] R. A. Durie and G. Herzberg, J. Chem. Phys. **38**, 806 (1960).
[26] I. Dabrowski and G. Herzberg, Can. J. Phys. **54**, 525 (1976).
[27] P. C. Hinnen, S. Werners, S. Stolte, W. Hogervorst, and W. Ubachs, Phys. Rev. A **52**, 4425 (1995).
[28] E. Reinhold, W. Hogervorst, and W. Ubachs, Chem. Phys. Lett. **296**, 411 (1998).
[29] W. Kołos, J. Mol. Spectrosc. **62**, 429 (1976).
[30] K. Dressler and L. Wolniewicz, Ber. Bunsenges. Phys. Chem. **99**, 246 (1995).
[31] Anonymous ftp to ftp.phys.uni.torun.pl/pub/publications/ifiz/luwo/bbhh_state.98.
[32] E. Reinhold, A. de Lange, W. Hogervorst, and W. Ubachs, J. Chem. Phys. **109**, 9772 (1998).
[33] P. C. Hinnen, W. Hogervorst, S. Stolte, and W. Ubachs, Can. J. Phys. **72**, 1032 (1994).
[34] E. Reinhold, W. Hogervorst, and W. Ubachs, J. Mol. Spectrosc. **180**, 156 (1996).
[35] S. Gerstenkorn and P. Luc, *Atlas du spectre d'absorption de la molécule d'iode* (CNRS, Paris, 1978).
[36] H. H. Li and C. J. Humphreys, J. Opt. Soc. Am. **64**, 1072 (1974).
[37] S. L. Bragg, J. W. Brault, and W. H. Smith, Astrophys. J. **263**, 999 (1982).
[38] P. Essenwanger and H. P. Gush, Can. J. Phys. **62**, 1680 (1984).
[39] A. R. W. McKellar and T. Oka, Can. J. Phys. **56**, 1315 (1978).
[40] T. Detmer, P. Schmelcher, and L. S. Cederbaum, J. Chem. Phys. **109**, 9694 (1998).